PROCEEDINGS OF SCIENCE

Measurements of Cloud Base Height and Coverage using Elastic Multiangle Lidar Scans at the Pierre Auger Observatory

Juan Vicente Pallotta[a] **and Jorge Ruben Rodriguez**[b,*] **for the Pierre Auger Collaboration**[b]

[a] *Centro de Investigaciones en Láseres y Aplicaciones, UNIDEF (CITEDEF-CONICET), Buenos Aires, Argentina.*

[b] *Observatorio Pierre Auger, Av. San Martín Norte 304, 5613 Malargüe, Argentina*
Full author list: https://www.auger.org/archive/authors_icrc_2023.html
E-mail: spokespersons@auger.org

Cloud features significantly affect the reconstruction of extensive air showers, and their characterization plays an important role in atmospheric monitoring. A multi-directional characterization of the cloud pattern is provided by a combination of several instruments of the atmospheric monitoring network at the Pierre Auger Observatory (Mendoza Province, Argentina). In this work, we present the results of an analysis of the cloud measurements using data taken from 2007 to 2022 by the elastic lidars positioned in the proximity of the fluorescence detector (FD) sites. These systems provide hourly measurements of cloud coverage and base height above FD. The ansatz of horizontal homogeneity of cloud structures is tested by comparing the hourly measurements of cloud base height and coverage done simultaneously at different lidar locations. These results allow a detailed description of cloud patterns observed above the array throughout the whole period. The variation of cloud parameters is shown and quantitative conclusions about cloud homogeneity across the array of the Pierre Auger Observatory are given.

38th International Cosmic Ray Conference (ICRC2023)
26 July - 3 August, 2023
Nagoya, Japan

*Speaker

1. Introduction

The Pierre Auger Observatory located in Malargue, Argentina (35.32S, 69.30W, 1416 m a.s.l.), is the largest hybrid cosmic-ray detector in the world. Its facilities combine a large array of water-Cherenkov detectors covering an area of 3000 km^2 and a fluorescence detector (FD) overlooking the surface array from different points of view. The FD stations, located at the sites of Los Leones (LL), Los Morados (LM), Loma Amarilla (LA), and Coihueco (CO), have 27 large telescopes aimed to detect the UV radiation produced by the interaction of the extensive air shower with nitrogen molecules in the Earth atmosphere. Their product accuracy relies on the atmospheric optical properties, which are subject to variations during the data taking. One of the major obstacles related to observation using FD telescopes are the clouds since they obscure the field of view of the telescopes.

The multiangle-elastic backscatter lidars [1] co-located at each FD station, are systems capable of producing aerosol profiles and cloud parameters in their line of sight. These measurements are meant to obtain the aerosol's extinction and cloud properties (base heights, coverage, and thickness). Central Laser Facility (CLF) and eXtra Laser Facility (XLF) [2] can return cloud heights as part of the aerosol profile determination for the application of the proper correction to air shower light profiles. Both facilities are based on a laser, firing 50 scheduled pulses four times per hour, at the center of the array, during the FD data-taking periods, measuring the scattered photons using each FD telescope. The retrieval of aerosol parameters is done with the Data Normalized Analysis [2], which compares hourly laser light profiles to a reference profile registered on a very clear night chosen for each year. Also, infra-red (IR) cloud cameras at the FD sites provide measures of cloud coverage in the FD telescope fields of view.

2. Elastic-multiangle lidar system at Pierre Auger Observatory

One of the components for the atmospheric monitoring is a set of four multiangle-elastic backscatter lidar stations, located at each of the FD sites. In Figure 1, a schematic layout of the Auger Observatory is shown, where surface detector stations are represented by the gray dots with the FD sites located at the borders of the array.

During the FD data collection, the lidars conduct regular scans of the sky outside the FD's field-of-view (FOV). For cloud-retrieval parameters (base/top height, thickness, coverage), continuous scans are performed, while discrete scans are used for optical retrieval of the aerosol. Also, hourly horizontal shots towards the pampa are used to measure the aerosol attenuation at ground level and the horizontal homogeneity, vetoing the acquisition of FD for 30 seconds every hour. This work focuses on cloud parameter retrieval, so continuous scan data are used. This scan type is performed in two orthogonal planes, firing laser pulses outside the field of view of the FDs. The data are analyzed to provide one measurement per hour, reporting the lowest cloud base height and the highest fraction of the sky covered with clouds within the hour. A new and more robust algorithm for cloud parameters retrieval is applied, based on a dynamic threshold instead of the differentials method used in a previous analysis.

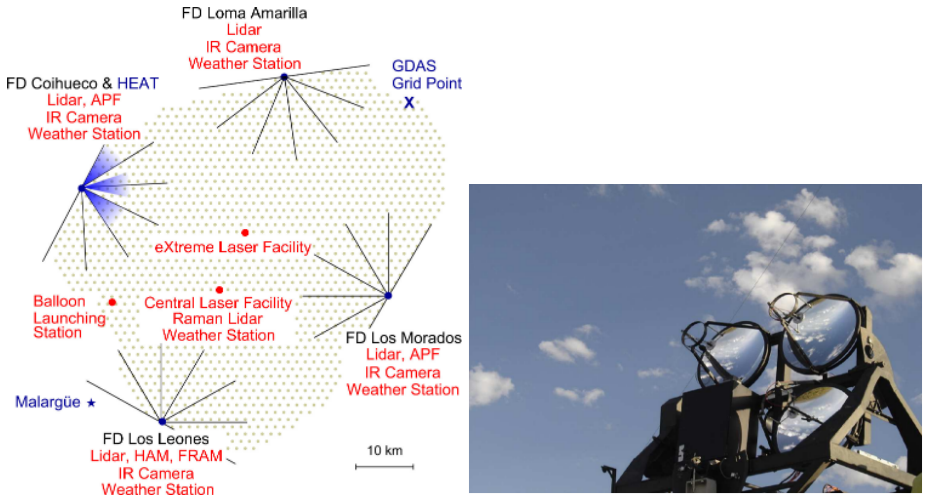

Figure 1: (a) Schematic layout of the Pierre Auger Observatory [3]. (b) Picture of one of the elastic-multiangle lidar systems.

3. Lidar cloud detection algorithm

Different cloud base/top height definitions can be found in the literature, and there is not a single algorithm suitable for all clouds [4], being also strongly influenced by the measuring instrument [5]. In the algorithm used to create this cloud database, no cloud/aerosol plumes are discriminated, and only the increased backscatter in the elastic-lidar signals is detected, also called a "feature" [6] or simply a "layer". Most used algorithms are differential-based methods like [5], relying on the differential of the range-corrected lidar signals (RCLS), dealing with the noise (especially at higher ranges). These methods depend strongly on the lidar features, and no universal algorithm/parameters are reported capable of working in any elastic lidar hardware and atmospheric scenario. Also, wavelengths close to the infra-red spectrum must be used for best performance, while the elastic-lidar from the Auger Observatory uses 351 nm. The algorithm applied to the elastic-multiangle Auger database is based on a dynamic threshold to detect the layer, showing excellent results for unattended analysis for big databases. The software used is the Lidar Processing Pipeline (LPP, [7]) developed and used in the Latin American lidar community.

A typical colormap image produced from continuous scans is shown in Figure 2a, where the RCLS are shown for better discrimination of the layer. RCLS is suitable for plotting since it removes the inverse-squared range dependence in the raw-lidar signal. Figure 2b shows the cloud mask retrieved from the data of Figure 2a, which shows the good performance on the cloud discrimination of the algorithm.

The algorithm produces the cloud features to be saved in the database, like the cloud-base height (CBH), cloud physical thickness (CT), cloud optical depth (COD), and cloud coverage (COV). COV is determined by the rate of the number of profiles with clouds and the total number of profiles within the scan:

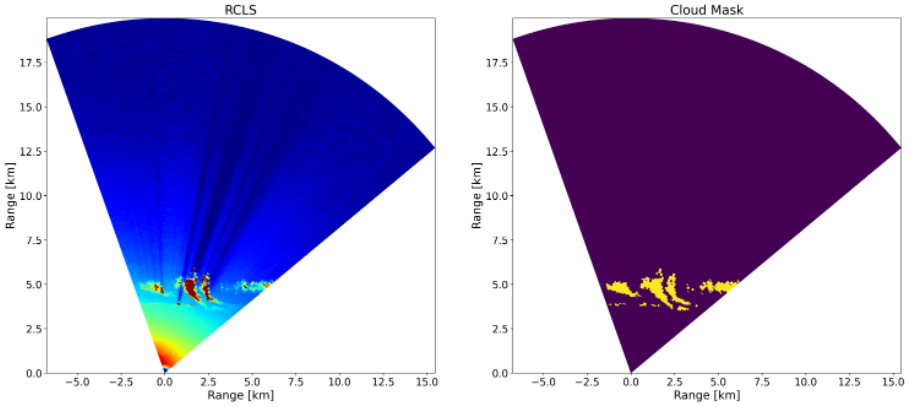

Figure 2: Example of multiangle continuous scan from the Coihueco site. The image is obtained summing about 100 profiles (1000 laser shots each), acquired in 10 minutes.

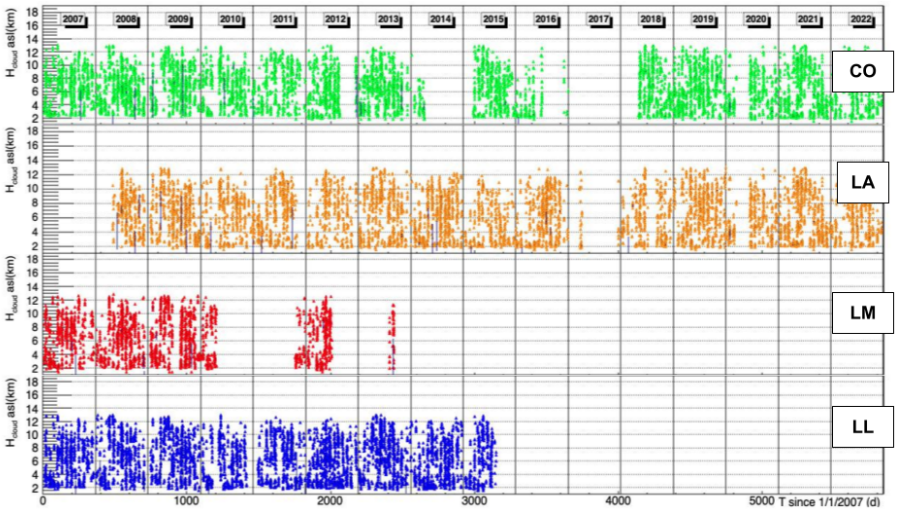

Figure 3: Cloud-base height generated with the new cloud retrieval algorithm for each site for the period 2007 until 2022.

$$COV = \frac{\#Lidar\ Profiles\ with\ Clouds}{\#Total\ Lidar\ Profiles\ of\ the\ Scan}.$$

Once the mentioned products are produced for each continuous scan, another software module merges the data hourly, retrieving the lowest cloud base height and the highest cloud coverage within the hour.

4. New cloud database

The new cloud retrieval algorithm was applied through the whole lidar data from 2007 to 2022 for all the sites. The cloud base height for the operational periods for each site is shown in Figure 3.

Site	Tot. Meas. Hours	COV $\leq$ 0.1 (COV=0)	0.1 < COV < 0.9	COV $\geq$ 0.9
LL	11256	43 % (42 %)	14 %	43 %
LM	5174	48 % (46 %)	15 %	37 %
LA	16293	53 % (51 %)	18 %	29 %
CO	17180	52 % (51 %)	17 %	31 %

Table 1: Cloud-coverage data for the whole period of analysis 2007-2022 for all the sites.

As can be seen in Figure 3, LL and LM sites discontinued their operation in 2015 and 2013 respectively. This makes the homogeneity analysis more relevant to extrapolate the lidar information into the field of view of the FD.

4.1 Cloud Coverage (COV) Rates Analysis

An overview of the data for each site is shown in Table 1, which summarizes the total amount of hours in the analyzed period (2007-2022) and the rates of different cloud coverage (COV) scenarios. These scenarios are described as low-COV rate (COV $\leq$ 0.1), high-COV rate (COV $\geq$ 0.9), and middle-COV rate (0.1 < COV < 0.9). The rates are calculated by dividing the number of events that meet the coverage condition by the total number of events that occurred during the entire period under analysis.

A mean of 49 % low-COV rates is found for all sites, meaning that half of the exposure time at the Observatory has only up to 10 % cloud coverage. The difference in the low-COV rate between all sites is $\pm$ 5 %.

The high-COV rates show a dispersion of 14 % between its maximum and minimum, and a mean of 35 %. These values show a predominance of low over high cloud coverage when the lidars are in operation. Nights characterized by a very low cloud layer, which reflects the lidar light in the FD telescope's FOV, are not included in this consideration as then the lidars are turned off to avoid interference with FD data taking. LA is the site with the best observation condition, showing the highest low-COV rate (53 %) and the lowest high-COV rate (29 %). On the other end, LL is the most cloudy site, with the lowest low-COV rate (43 %) and the highest high-COV rate (43 %).

4.2 Quarterly cloud base height (CBH) Histograms

In Figure 4 the percentage of occurrence of each CBH is shown, without accounting for the cloudless condition.

All sites show similar behavior within each trimester with two predominance modes except for the warmer trimester (January to March). Also, a predominance of low clouds (< 5 km) is seen for all the sites during the year, having their maximum peak in the summer (around 15 % for all the sites). For clouds between 5 and 10 km, no significant differences are seen from April to December, having a mean percentage ranging from 4 to 5 %. Winter months show less difference in the peaks of the two modes, showing a more homogeneous CBH distribution than in the summer. Another feature that can be spotted in Figure 4 is the increased number of clouds between 4-5 km at CO during the coldest trimesters (April to September) due to the effects of the Andes mountain.

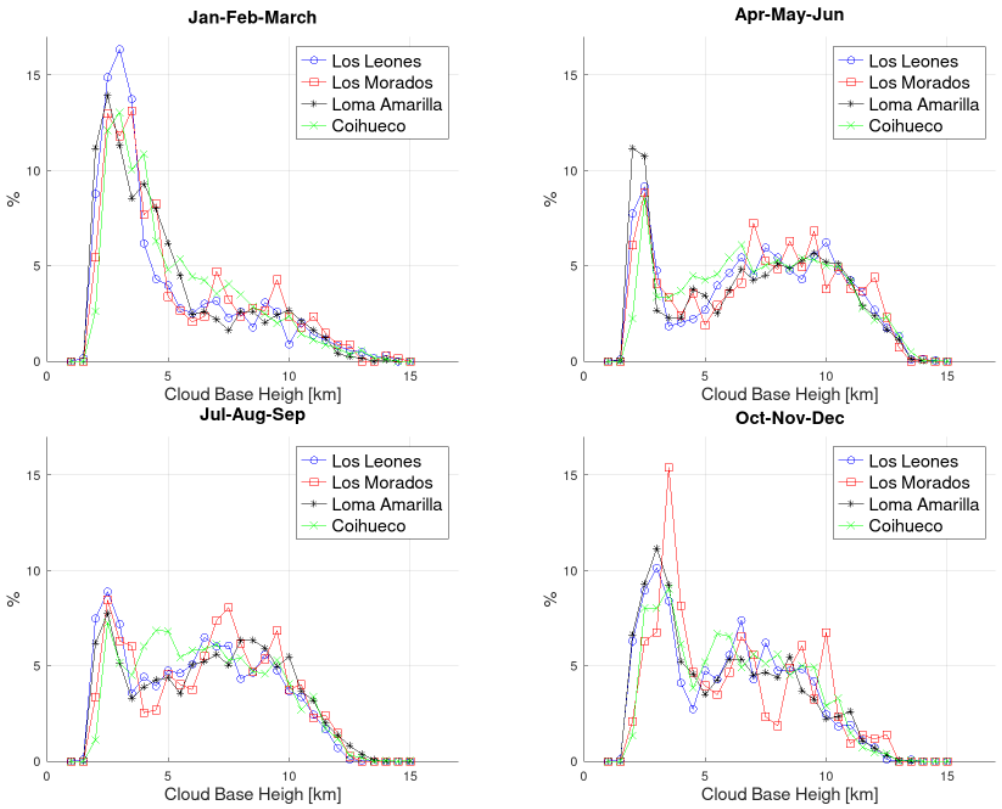

Figure 4: Cloud-base height distributions clustered by trimesters a the year.

5. Homogeneity analysis

In the homogeneity analysis, the cloud parameter of two different sites are compared in time-coincidence. The data on cross-correlations between sites was used to assess the horizontal homogeneity of the highland where the observatory is located. Data are compared on two observables: cloud base height and cloud coverage. While elastic lidars can detect multiple layers of clouds, only the base height of the lowest one is currently saved in our database.

5.1 COV percentages of coincidence

The rate at which a certain cloud coverage range is observed at two sites simultaneously is referred to as the "cloud coverage coincidence rate". For this analysis, cloudless situations are not taken into account. The expression of this rate can be expressed exemplarily for the low cloud scenario (COV ≤ 0.1) can be expressed as:

$$COV\ Percentage\ of\ Coincidence(COV \leq 0.1) = 100\,x\,\frac{\#[(Site_1\ \&\ Site_2) \rightarrow COV \leq 0.1]}{\#[Total\ Cloud\ Coincidence\ Events]}.$$

Applying the equation for each of the six combinations and clustering the comparison for COV $\leq$ 0.1 and COV $\geq$ 0.9, we obtain the Table 2.

	LL	LM	LA	CO	
LL	X	28 %	23 %	24 %	COV ≥ 0.9 on both sites
LM	36 %	X	22 %	23 %	
LA	34 %	38 %	X	19 %	
CO	39 %	39 %	44 %	X	
	COV ≤ 0.1 on both sites				

Table 2: COV percentage of coincidence for coverages lower than 0.1 and higher than 0.9 on both sites.

The lower-left/upper-right segment of Table 2 shows the low-COV/high-COV percentages of coincidence. The percentage span for low and high COV are similar: 10 % and 9 %, having mean values of 38 % for low-COV and 23 % for high-COV. From these values, it can be concluded that under low cloud coverage, (COV ≤ 0.1), CO and LA (the closest sites, separated by ∼ 40.7 km) show the highest percentage of coincidence (44 %), and LA and LL show the lowest percentage of coincidence (34 %). The latter is a somehow predictable situation since LA and LL are the most separated sites in the field (∼65.7 km) and it is not expected to have a similar cloud scenario if both see few clouds. These results are in concordance with the values of Table 1, where CO and LA show both quite high and very similar percentages of low coverage (52 % and 53 % respectively) and LA and LL have the largest difference in the COV feature (53 % and 43 % respectively).

Under a high-cloud scenario (COV ≥ 0.9, upper-right part of the Table 2), CO and LA have the lowest percentage of coincidence (19 %), despite the fact that they are the closest sites. This is because LA is the site with the lowest cloud coverage (see Table 1) and CO is influenced by the turbulence downwind with respect to the Andes, having a different development of the clouds over its site. LL and LM have the highest percentage of coincidence (28 %) under this cloud coverage scenario. Previous studies conducted by the Auger Collaboration [8] and [9] have identified these two locations within the array as the most aerosol-loaded ones, potentially serving as the origin of particles for the condensation nuclei for cloud formation. These results are also confirmed with the values of Table 1, in which LL and LM are the most cloudy sites in the array.

5.2 CBH percentage of coincidence

Cloud-base height percentage of coincidence is processed when the two sites under comparison have clouds. The expression to calculate the percentage of coincidence when the CBH ≤ 5 km can be expressed as:

$$CBH\,Percentage\,of\,Coincidence\,(CBH \leq 5km) = 100x\,\frac{\#[(Site_1\ \&\ Site_2) \rightarrow CBH \leq 5km]}{\#[Total\ Cloud\ Coincidence\ Events]}.$$

The comparison between each site and the respective percentages are shown in Table 3.

The lower-left/upper-right part of Table 3 shows the coincidence percentage when both sites show a cloud-base height lower (L_{ij})/higher (H_{ij}) than 5 km at the same time. The span of the coincidence's percentage are 6 % and 4 % for both clusters.

	LL	LM	LA	CO	
LL	X	55 %	55 %	58 %	H_{ij}:CBH > 5 km on both sites
LM	30 %	X	59 %	57 %	
LA	28 %	28 %	X	55 %	
CO	26 %	24 %	30 %	X	
	L_{ij}:CBH ≤ 5 km on both sites				

Table 3: Cloud base height percentage of coincidence when the two sites see clouds base height lower (L_{ij})/higher (H_{ij}) than 5 km.

For each pair of sites, the fraction $F_{ij} = 1 - L_{ij} - H_{ij}$, complementary to the ones listed in the table allows us to quantify the condition of maximal inhomogeneity, i.e. when one site has clouds below 5 km and the other has high clouds. We conclude that the LM-LA pair is the one with minimal inhomogeneity (13 %) and LM-CO is the one with maximum inhomogeneity (19 %). CO has the lowest inhomogeneity with LL (16 %). This information can be used to guess the cloud scenario for the sites in which there is no lidar data today: LL and LM with the data of CO and LA respectively.

6. Conclusion

The elastic lidar network is a key component of the atmospheric monitoring system of the Pierre Auger Observatory, which provides information on the cloud pattern above each FD site during regular data-taking operations. In this work, we use a more robust automatic cloud retrieval algorithm, to extract the cloud parameters like the cloud-base height and cloud coverage (among others), and we describe a general method to statistically extend the validity of our measurements to the sites where the harsh conditions of operation have forced the shutdown of our instruments.

References

[1] BenZvi S. et al., NIM A574, (2007) 171.

[2] The Pierre Auger Collaboration, JINST 8 (2013) 04009.

[3] A. Aab *et al.* Nucl. Instrum. Meth. A, **79** (2015) 172.

[4] Platt C et al., 1994, Bull. Amer. Meteor. Soc. **75** (1994) 1635.

[5] Pal S et. al., 1992, Appl. Opt. **31** (1992) 1488.

[6] Vaughan M. et. al., Journal of Atmospheric and Oceanic Technology **26** (2009) 2034.

[7] Pallotta, J. V. *et al.* , https://gi.copernicus.org/preprints/gi-2022-19/ (2022).

[8] S. Ben Zvi *et al.* [Pierre Auger], [arXiv:0706.3236 [astro-ph]].

[9] A. Aab *et al.* [Pierre Auger Collaboration], Atmos. Res. **149** (2014) 120.

The Pierre Auger Collaboration

A. Abdul Halim[13], P. Abreu[72], M. Aglietta[54,52], I. Allekotte[1], K. Almeida Cheminant[70], A. Almela[7,12], R. Aloisio[45,46], J. Alvarez-Muñiz[79], J. Ammerman Yebra[79], G.A. Anastasi[54,52], L. Anchordoqui[86], B. Andrada[7], S. Andringa[72], C. Aramo[50], P.R. Araújo Ferreira[42], E. Arnone[63,52], J. C. Arteaga Velázquez[67], H. Asorey[7], P. Assis[72], G. Avila[11], E. Avocone[57,46], A.M. Badescu[75], A. Bakalova[32], A. Balaceanu[73], F. Barbato[45,46], A. Bartz Mocellin[85], J.A. Bellido[13,69], C. Berat[36], M.E. Bertaina[63,52], G. Bhatta[70], M. Bianciotto[63,52], P.L. Biermann[h], V. Binet[5], K. Bismark[39,7], T. Bister[80,81], J. Biteau[37], J. Blazek[32], C. Bleve[36], J. Blümer[41], M. Boháčová[32], D. Boncioli[57,46], C. Bonifazi[8,26], L. Bonneau Arbeletche[21], N. Borodai[70], J. Brack[j], P.G. Brichetto Orchera[7], F.L. Briechle[42], A. Bueno[78], S. Buitink[15], M. Buscemi[47,61], M. Büsken[39,7], A. Bwembya[80,81], K.S. Caballero-Mora[66], S. Cabana-Freire[79], L. Caccianiga[59,49], I. Caracas[38], R. Caruso[58,47], A. Castellina[54,52], F. Catalani[18], G. Cataldi[48], L. Cazon[79], M. Cerda[10], A. Cermenati[45,46], J.A. Chinellato[21], J. Chudoba[32], L. Chytka[33], R.W. Clay[13], A.C. Cobos Cerutti[6], R. Colalillo[60,50], A. Coleman[90], M.R. Coluccia[48], R. Conceição[72], A. Condorelli[37], G. Consolati[49,55], M. Conte[56,48], F. Convenga[41], D. Correia dos Santos[28], P.J. Costa[72], C.E. Covault[84], M. Cristinziani[44], C.S. Cruz Sanchez[3], S. Dasso[4,2], K. Daumiller[41], B.R. Dawson[13], R.M. de Almeida[28], J. de Jesús[7,41], S.J. de Jong[80,81], J.R.T. de Mello Neto[26,27], I. De Mitri[45,46], J. de Oliveira[17], D. de Oliveira Franco[21], F. de Palma[56,48], V. de Souza[19], E. De Vito[56,48], A. Del Popolo[58,47], O. Deligny[34], N. Denner[32], L. Deval[41,7], A. di Matteo[52], M. Dobre[73], C. Dobrigkeit[21], J.C. D'Olivo[68], L.M. Domingues Mendes[72], J.C. dos Anjos, R.C. dos Anjos[25], J. Ebr[32], F. Ellwanger[41], M. Emam[80,81], R. Engel[39,41], I. Epicoco[56,48], M. Erdmann[42], A. Etchegoyen[7,12], C. Evoli[45,46], H. Falcke[80,82,81], J. Farmer[89], G. Farrar[88], A.C. Fauth[21], N. Fazzini[e], F. Feldbusch[40], F. Fenu[41,d], A. Fernandes[72], B. Fick[87], J.M. Figueira[7], A. Filipčič[77,76], T. Fitoussi[41], B. Flaggs[90], T. Fodran[80], T. Fujii[89,f], A. Fuster[7,12], C. Galea[80], C. Galelli[59,49], B. García[6], C. Gaudu[38], H. Gemmeke[40], F. Gesualdi[7,41], A. Gherghel-Lascu[73], P.L. Ghia[34], U. Giaccari[48], M. Giammarchi[49], J. Glombitza[42,g], F. Gobbi[10], F. Gollan[7], G. Golup[1], M. Gómez Berisso[1], P.F. Gómez Vitale[11], J.P. Gongora[11], J.M. González[1], N. González[7], I. Goos[1], D. Góra[70], A. Gorgi[54,52], M. Gottowik[79], T.D. Grubb[13], F. Guarino[60,50], G.P. Guedes[22], E. Guido[44], S. Hahn[39], P. Hamal[32], M.R. Hampel[7], P. Hansen[3], D. Harari[1], V.M. Harvey[13], A. Haungs[41], T. Hebbeker[42], C. Hojvat[e], J.R. Hörandel[80,81], P. Horvath[33], M. Hrabovský[33], T. Huege[41,15], A. Insolia[58,47], P.G. Isar[74], P. Janecek[32], J.A. Johnsen[85], J. Jurysek[32], A. Kääpä[38], K.H. Kampert[38], B. Keilhauer[41], A. Khakurdikar[80], V.V. Kizakke Covilakam[7,41], H.O. Klages[41], M. Kleifges[40], F. Knapp[39], N. Kunka[40], B.L. Lago[16], N. Langner[42], M.A. Leigui de Oliveira[24], Y Lema-Capeans[79], V. Lenok[39], A. Letessier-Selvon[35], I. Lhenry-Yvon[34], D. Lo Presti[58,47], L. Lopes[72], L. Lu[91], Q. Luce[39], J.P. Lundquist[76], A. Machado Payeras[21], M. Majercakova[32], D. Mandat[32], B.C. Manning[13], P. Mantsch[e], S. Marafico[34], F.M. Mariani[59,49], A.G. Mariazzi[3], I.C. Mariş[14], G. Marsella[61,47], D. Martello[56,48], S. Martinelli[41,7], O. Martínez Bravo[64], M.A. Martins[79], M. Mastrodicasa[57,46], H.J. Mathes[41], J. Matthews[a], G. Matthiae[62,51], E. Mayotte[85,38], S. Mayotte[85], P.O. Mazur[e], G. Medina-Tanco[68], J. Meinert[38], D. Melo[7], A. Menshikov[40], C. Merx[41], S. Michal[33], M.I. Micheletti[5], L. Miramonti[59,49], S. Mollerach[1], F. Montanet[36], L. Morejon[38], C. Morello[54,52], A.L. Müller[32], K. Mulrey[80,81], R. Mussa[52], M. Muzio[88], W.M. Namasaka[38], S. Negi[32], L. Nellen[68], K. Nguyen[87], G. Nicora[9], M. Niculescu-Oglinzanu[73], M. Niechciol[44], D. Nitz[87], D. Nosek[31], V. Novotny[31], L. Nožka[33], A Nucita[56,48], L.A. Núñez[30], C. Oliveira[19], M. Palatka[32], J. Pallotta[9], S. Panja[32], G. Parente[79], T. Paulsen[38], J. Pawlowsky[38], M. Pech[32], J. Pękala[70], R. Pelayo[65], L.A.S. Pereira[23], E.E. Pereira Martins[39,7], J. Perez Armand[20], C. Pérez Bertolli[7,41], L. Perrone[56,48], S. Petrera[45,46], C. Petrucci[57,46], T. Pierog[41], M. Pimenta[72], M. Platino[7], B. Pont[80], M. Pothast[81,80], M. Pourmohammad Shahvar[61,47], P. Privitera[89], M. Prouza[32], A. Puyleart[87], S. Querchfeld[38], J. Rautenberg[38], D. Ravignani[7], M. Reininghaus[39], J. Ridky[32], F. Riehn[79], M. Risse[44], V. Rizi[57,46], W. Rodrigues de Carvalho[80], E. Rodriguez[7,41], J. Rodriguez Rojo[11], M.J. Roncoroni[7], S. Rossoni[43], M. Roth[41], E. Roulet[1], A.C. Rovero[4], P. Ruehl[44], A. Saftoiu[73], M. Saharan[80], F. Salamida[57,46], H. Salazar[64], G. Salina[51], J.D. Sanabria Gomez[30], F. Sánchez[7], E.M. Santos[20], E. Santos[32],

F. Sarazin[85], R. Sarmento[72], R. Sato[11], P. Savina[91], C.M. Schäfer[41], V. Scherini[56,48], H. Schieler[41], M. Schimassek[34], M. Schimp[38], F. Schlüter[41], D. Schmidt[39], O. Scholten[15,*i*], H. Schoorlemmer[80,81], P. Schovánek[32], F.G. Schröder[90,41], J. Schulte[42], T. Schulz[41], S.J. Sciutto[3], M. Scornavacche[7,41], A. Segreto[53,47], S. Sehgal[38], S.U. Shivashankara[76], G. Sigl[43], G. Silli[7], O. Sima[73,*b*], F. Simon[40], R. Smau[73], R. Šmída[89], P. Sommers[*k*], J.F. Soriano[86], R. Squartini[10], M. Stadelmaier[32], D. Stanca[73], S. Stanič[76], J. Stasielak[70], P. Stassi[36], S. Strähnz[39], M. Straub[42], M. Suárez-Durán[14], T. Suomijärvi[37], A.D. Supanitsky[7], Z. Svozilikova[32], Z. Szadkowski[71], A. Tapia[29], C. Taricco[63,52], C. Timmermans[81,80], O. Tkachenko[41], P. Tobiska[32], C.J. Todero Peixoto[18], B. Tomé[72], Z. Torrès[36], A. Travaini[10], P. Travnicek[32], C. Trimarelli[57,46], M. Tueros[3], M. Unger[41], L. Vaclavek[33], M. Vacula[33], J.F. Valdés Galicia[68], L. Valore[60,50], E. Varela[64], A. Vásquez-Ramírez[30], D. Veberič[41], C. Ventura[27], I.D. Vergara Quispe[3], V. Verzi[51], J. Vicha[32], J. Vink[83], J. Vlastimil[32], S. Vorobiov[76], C. Watanabe[26], A.A. Watson[*c*], A. Weindl[41], L. Wiencke[85], H. Wilczyński[70], D. Wittkowski[38], B. Wundheiler[7], B. Yue[38], A. Yushkov[32], O. Zapparrata[14], E. Zas[79], D. Zavrtanik[76,77], M. Zavrtanik[77,76]

———— • ————

[1] Centro Atómico Bariloche and Instituto Balseiro (CNEA-UNCuyo-CONICET), San Carlos de Bariloche, Argentina
[2] Departamento de Física and Departamento de Ciencias de la Atmósfera y los Océanos, FCEyN, Universidad de Buenos Aires and CONICET, Buenos Aires, Argentina
[3] IFLP, Universidad Nacional de La Plata and CONICET, La Plata, Argentina
[4] Instituto de Astronomía y Física del Espacio (IAFE, CONICET-UBA), Buenos Aires, Argentina
[5] Instituto de Física de Rosario (IFIR) – CONICET/U.N.R. and Facultad de Ciencias Bioquímicas y Farmacéuticas U.N.R., Rosario, Argentina
[6] Instituto de Tecnologías en Detección y Astropartículas (CNEA, CONICET, UNSAM), and Universidad Tecnológica Nacional – Facultad Regional Mendoza (CONICET/CNEA), Mendoza, Argentina
[7] Instituto de Tecnologías en Detección y Astropartículas (CNEA, CONICET, UNSAM), Buenos Aires, Argentina
[8] International Center of Advanced Studies and Instituto de Ciencias Físicas, ECyT-UNSAM and CONICET, Campus Miguelete – San Martín, Buenos Aires, Argentina
[9] Laboratorio Atmósfera – Departamento de Investigaciones en Láseres y sus Aplicaciones – UNIDEF (CITEDEF-CONICET), Argentina
[10] Observatorio Pierre Auger, Malargüe, Argentina
[11] Observatorio Pierre Auger and Comisión Nacional de Energía Atómica, Malargüe, Argentina
[12] Universidad Tecnológica Nacional – Facultad Regional Buenos Aires, Buenos Aires, Argentina
[13] University of Adelaide, Adelaide, S.A., Australia
[14] Université Libre de Bruxelles (ULB), Brussels, Belgium
[15] Vrije Universiteit Brussels, Brussels, Belgium
[16] Centro Federal de Educação Tecnológica Celso Suckow da Fonseca, Petropolis, Brazil
[17] Instituto Federal de Educação, Ciência e Tecnologia do Rio de Janeiro (IFRJ), Brazil
[18] Universidade de São Paulo, Escola de Engenharia de Lorena, Lorena, SP, Brazil
[19] Universidade de São Paulo, Instituto de Física de São Carlos, São Carlos, SP, Brazil
[20] Universidade de São Paulo, Instituto de Física, São Paulo, SP, Brazil
[21] Universidade Estadual de Campinas, IFGW, Campinas, SP, Brazil
[22] Universidade Estadual de Feira de Santana, Feira de Santana, Brazil
[23] Universidade Federal de Campina Grande, Centro de Ciencias e Tecnologia, Campina Grande, Brazil
[24] Universidade Federal do ABC, Santo André, SP, Brazil
[25] Universidade Federal do Paraná, Setor Palotina, Palotina, Brazil
[26] Universidade Federal do Rio de Janeiro, Instituto de Física, Rio de Janeiro, RJ, Brazil
[27] Universidade Federal do Rio de Janeiro (UFRJ), Observatório do Valongo, Rio de Janeiro, RJ, Brazil
[28] Universidade Federal Fluminense, EEIMVR, Volta Redonda, RJ, Brazil
[29] Universidad de Medellín, Medellín, Colombia
[30] Universidad Industrial de Santander, Bucaramanga, Colombia
[31] Charles University, Faculty of Mathematics and Physics, Institute of Particle and Nuclear Physics, Prague, Czech

Republic
[32] Institute of Physics of the Czech Academy of Sciences, Prague, Czech Republic
[33] Palacky University, Olomouc, Czech Republic
[34] CNRS/IN2P3, IJCLab, Université Paris-Saclay, Orsay, France
[35] Laboratoire de Physique Nucléaire et de Hautes Energies (LPNHE), Sorbonne Université, Université de Paris, CNRS-IN2P3, Paris, France
[36] Univ. Grenoble Alpes, CNRS, Grenoble Institute of Engineering Univ. Grenoble Alpes, LPSC-IN2P3, 38000 Grenoble, France
[37] Université Paris-Saclay, CNRS/IN2P3, IJCLab, Orsay, France
[38] Bergische Universität Wuppertal, Department of Physics, Wuppertal, Germany
[39] Karlsruhe Institute of Technology (KIT), Institute for Experimental Particle Physics, Karlsruhe, Germany
[40] Karlsruhe Institute of Technology (KIT), Institut für Prozessdatenverarbeitung und Elektronik, Karlsruhe, Germany
[41] Karlsruhe Institute of Technology (KIT), Institute for Astroparticle Physics, Karlsruhe, Germany
[42] RWTH Aachen University, III. Physikalisches Institut A, Aachen, Germany
[43] Universität Hamburg, II. Institut für Theoretische Physik, Hamburg, Germany
[44] Universität Siegen, Department Physik – Experimentelle Teilchenphysik, Siegen, Germany
[45] Gran Sasso Science Institute, L'Aquila, Italy
[46] INFN Laboratori Nazionali del Gran Sasso, Assergi (L'Aquila), Italy
[47] INFN, Sezione di Catania, Catania, Italy
[48] INFN, Sezione di Lecce, Lecce, Italy
[49] INFN, Sezione di Milano, Milano, Italy
[50] INFN, Sezione di Napoli, Napoli, Italy
[51] INFN, Sezione di Roma "Tor Vergata", Roma, Italy
[52] INFN, Sezione di Torino, Torino, Italy
[53] Istituto di Astrofisica Spaziale e Fisica Cosmica di Palermo (INAF), Palermo, Italy
[54] Osservatorio Astrofisico di Torino (INAF), Torino, Italy
[55] Politecnico di Milano, Dipartimento di Scienze e Tecnologie Aerospaziali , Milano, Italy
[56] Università del Salento, Dipartimento di Matematica e Fisica "E. De Giorgi", Lecce, Italy
[57] Università dell'Aquila, Dipartimento di Scienze Fisiche e Chimiche, L'Aquila, Italy
[58] Università di Catania, Dipartimento di Fisica e Astronomia "Ettore Majorana", Catania, Italy
[59] Università di Milano, Dipartimento di Fisica, Milano, Italy
[60] Università di Napoli "Federico II", Dipartimento di Fisica "Ettore Pancini", Napoli, Italy
[61] Università di Palermo, Dipartimento di Fisica e Chimica "E. Segrè", Palermo, Italy
[62] Università di Roma "Tor Vergata", Dipartimento di Fisica, Roma, Italy
[63] Università Torino, Dipartimento di Fisica, Torino, Italy
[64] Benemérita Universidad Autónoma de Puebla, Puebla, México
[65] Unidad Profesional Interdisciplinaria en Ingeniería y Tecnologías Avanzadas del Instituto Politécnico Nacional (UPIITA-IPN), México, D.F., México
[66] Universidad Autónoma de Chiapas, Tuxtla Gutiérrez, Chiapas, México
[67] Universidad Michoacana de San Nicolás de Hidalgo, Morelia, Michoacán, México
[68] Universidad Nacional Autónoma de México, México, D.F., México
[69] Universidad Nacional de San Agustin de Arequipa, Facultad de Ciencias Naturales y Formales, Arequipa, Peru
[70] Institute of Nuclear Physics PAN, Krakow, Poland
[71] University of Łódź, Faculty of High-Energy Astrophysics,Łódź, Poland
[72] Laboratório de Instrumentação e Física Experimental de Partículas – LIP and Instituto Superior Técnico – IST, Universidade de Lisboa – UL, Lisboa, Portugal
[73] "Horia Hulubei" National Institute for Physics and Nuclear Engineering, Bucharest-Magurele, Romania
[74] Institute of Space Science, Bucharest-Magurele, Romania
[75] University Politehnica of Bucharest, Bucharest, Romania
[76] Center for Astrophysics and Cosmology (CAC), University of Nova Gorica, Nova Gorica, Slovenia
[77] Experimental Particle Physics Department, J. Stefan Institute, Ljubljana, Slovenia
[78] Universidad de Granada and C.A.F.P.E., Granada, Spain

[79] Instituto Galego de Física de Altas Enerxías (IGFAE), Universidade de Santiago de Compostela, Santiago de Compostela, Spain
[80] IMAPP, Radboud University Nijmegen, Nijmegen, The Netherlands
[81] Nationaal Instituut voor Kernfysica en Hoge Energie Fysica (NIKHEF), Science Park, Amsterdam, The Netherlands
[82] Stichting Astronomisch Onderzoek in Nederland (ASTRON), Dwingeloo, The Netherlands
[83] Universiteit van Amsterdam, Faculty of Science, Amsterdam, The Netherlands
[84] Case Western Reserve University, Cleveland, OH, USA
[85] Colorado School of Mines, Golden, CO, USA
[86] Department of Physics and Astronomy, Lehman College, City University of New York, Bronx, NY, USA
[87] Michigan Technological University, Houghton, MI, USA
[88] New York University, New York, NY, USA
[89] University of Chicago, Enrico Fermi Institute, Chicago, IL, USA
[90] University of Delaware, Department of Physics and Astronomy, Bartol Research Institute, Newark, DE, USA
[91] University of Wisconsin-Madison, Department of Physics and WIPAC, Madison, WI, USA

—

[a] Louisiana State University, Baton Rouge, LA, USA
[b] also at University of Bucharest, Physics Department, Bucharest, Romania
[c] School of Physics and Astronomy, University of Leeds, Leeds, United Kingdom
[d] now at Agenzia Spaziale Italiana (ASI). Via del Politecnico 00133, Roma, Italy
[e] Fermi National Accelerator Laboratory, Fermilab, Batavia, IL, USA
[f] now at Graduate School of Science, Osaka Metropolitan University, Osaka, Japan
[g] now at ECAP, Erlangen, Germany
[h] Max-Planck-Institut für Radioastronomie, Bonn, Germany
[i] also at Kapteyn Institute, University of Groningen, Groningen, The Netherlands
[j] Colorado State University, Fort Collins, CO, USA
[k] Pennsylvania State University, University Park, PA, USA

Acknowledgments

The successful installation, commissioning, and operation of the Pierre Auger Observatory would not have been possible without the strong commitment and effort from the technical and administrative staff in Malargüe. We are very grateful to the following agencies and organizations for financial support:

Argentina – Comisión Nacional de Energía Atómica; Agencia Nacional de Promoción Científica y Tecnológica (ANPCyT); Consejo Nacional de Investigaciones Científicas y Técnicas (CONICET); Gobierno de la Provincia de Mendoza; Municipalidad de Malargüe; NDM Holdings and Valle Las Leñas; in gratitude for their continuing cooperation over land access; Australia – the Australian Research Council; Belgium – Fonds de la Recherche Scientifique (FNRS); Research Foundation Flanders (FWO); Brazil – Conselho Nacional de Desenvolvimento Científico e Tecnológico (CNPq); Financiadora de Estudos e Projetos (FINEP); Fundação de Amparo à Pesquisa do Estado de Rio de Janeiro (FAPERJ); São Paulo Research Foundation (FAPESP) Grants No. 2019/10151-2, No. 2010/07359-6 and No. 1999/05404-3; Ministério da Ciência, Tecnologia, Inovações e Comunicações (MCTIC); Czech Republic – Grant No. MSMT CR LTT18004, LM2015038, LM2018102, CZ.02.1.01/0.0/0.0/16_013/0001402, CZ.02.1.01/0.0/0.0/18_046/0016010 and CZ.02.1.01/0.0/0.0/17_049/0008422; France – Centre de Calcul IN2P3/CNRS; Centre National de la Recherche Scientifique (CNRS); Conseil Régional Ile-de-France; Département Physique Nucléaire et Corpusculaire (PNC-IN2P3/CNRS); Département Sciences de l'Univers (SDU-INSU/CNRS); Institut Lagrange de Paris (ILP) Grant No. LABEX ANR-10-LABX-63 within the Investissements d'Avenir Programme Grant No. ANR-11-IDEX-0004-02; Germany – Bundesministerium für Bildung und Forschung (BMBF); Deutsche Forschungsgemeinschaft (DFG); Finanzministerium Baden-Württemberg; Helmholtz Alliance for Astroparticle Physics (HAP); Helmholtz-Gemeinschaft Deutscher Forschungszentren (HGF); Ministerium für Kultur und Wissenschaft des Landes Nordrhein-Westfalen; Ministerium für Wissenschaft, Forschung und Kunst des Landes Baden-Württemberg; Italy – Istituto Nazionale di Fisica Nucleare (INFN); Istituto Nazionale di Astrofisica (INAF); Ministero dell'Universitá e della Ricerca (MUR); CETEMPS Center of Excellence; Ministero degli Affari Esteri (MAE), ICSC Centro Nazionale di Ricerca in High Performance Computing, Big Data and Quantum Computing, funded by European Union NextGenerationEU, reference code CN_00000013; México –

Consejo Nacional de Ciencia y Tecnología (CONACYT) No. 167733; Universidad Nacional Autónoma de México (UNAM); PAPIIT DGAPA-UNAM; The Netherlands – Ministry of Education, Culture and Science; Netherlands Organisation for Scientific Research (NWO); Dutch national e-infrastructure with the support of SURF Cooperative; Poland – Ministry of Education and Science, grants No. DIR/WK/2018/11 and 2022/WK/12; National Science Centre, grants No. 2016/22/M/ST9/00198, 2016/23/B/ST9/01635, 2020/39/B/ST9/01398, and 2022/45/B/ST9/02163; Portugal – Portuguese national funds and FEDER funds within Programa Operacional Factores de Competitividade through Fundação para a Ciência e a Tecnologia (COMPETE); Romania – Ministry of Research, Innovation and Digitization, CNCS-UEFISCDI, contract no. 30N/2023 under Romanian National Core Program LAPLAS VII, grant no. PN 23 21 01 02 and project number PN-III-P1-1.1-TE-2021-0924/TE57/2022, within PNCDI III; Slovenia – Slovenian Research Agency, grants P1-0031, P1-0385, I0-0033, N1-0111; Spain – Ministerio de Economía, Industria y Competitividad (FPA2017-85114-P and PID2019-104676GB-C32), Xunta de Galicia (ED431C 2017/07), Junta de Andalucía (SOMM17/6104/UGR, P18-FR-4314) Feder Funds, RENATA Red Nacional Temática de Astropartículas (FPA2015-68783-REDT) and María de Maeztu Unit of Excellence (MDM-2016-0692); USA – Department of Energy, Contracts No. DE-AC02-07CH11359, No. DE-FR02-04ER41300, No. DE-FG02-99ER41107 and No. DE-SC0011689; National Science Foundation, Grant No. 0450696; The Grainger Foundation; Marie Curie-IRSES/EPLANET; European Particle Physics Latin American Network; and UNESCO.